Temperature dependence of water self-diffusivity in pure polycrystalline ice and in ice doped with HCl: Fast thermal desorption spectroscopy study

Haiping Lu, Stephanie A. McCartney, and Vlad Sadtchenko*

Department of Chemistry
The George Washington University

DRAFT

*Corresponding author; Chemistry Department, The George Washington University, 725 21st St. NW, Rm. 107, Washington, DC 20052; phone: 202-994-6155; e-mail: vlad@gwu.edu

Abstract

We report the results of a fast thermal desorption spectroscopy study of the H/D isotopic exchange kinetics in a few micrometer thick, pure polycrystalline ice film and in ice films doped with HCl. Using the isotopic exchange reaction as a probe of molecular transport in ice, we were able to determine the effective water-self diffusion coefficients, D_{eff}, in pure and doped polycrystalline ice at temperatures ranging from -18 to -1 °C. In the case of pure polycrystalline, D_{eff} demonstrates an Arrhenius dependence on temperature with an effective activation energy of 69 ± 3 kJ·mol^{-1} and a pre-exponential of $10^{9\pm0.5}$ μm^2·ms^{-1} up to -2 °C. According to our analysis, the self-diffusion coefficient of water at the grain boundaries also shows an Arrhenius dependence on temperature with an activation energy of 69 ± 3 kJ·mol^{-1} and pre-exponential of $10^{11\pm1}$ μm^2·ms^{-1}. However, upon the addition of 0.04% of HCl into the polycrystalline ice results in a marked deviation of D_{eff} from Arrhenius law at -8 °C, which we attribute to

premelting, which takes place intersections of grain boundaries. We discuss structure and transport properties of condensed aqueous phase at grain boundaries in polycrystalline ice at various temperatures.

I. INTRODUCTION

Ice plays a crucial role in a variety of environmentally relevant processes such as frost heave, glacier motion, growth and decay of sea ice, dynamics of polar ice caps, chemical processing of pollutants in the atmosphere, water purification and desalination by freezing, and analysis of ice cores climate proxies[1-21]. Despite centuries of scientific inquires fundamental chemical and physical properties, water and ice remain poorly understood. The lack of fundamental understanding of chemical and physical phenomena which occur in the condensed aqueous phase has a negative impact on progress in many applied fields. In the current article, we report the results of our ongoing experimental investigation into the transport properties of the aqueous phase confined to the grain boundaries of fine polycrystalline ice at temperatures near its melting point.

Due to the extremely low solubility of most molecular species in single crystal ice samples, the grain boundaries (GB's) in polycrystalline ice samples serve as the primary storage and reaction sites for chemical impurities. Therefore, an understanding of the bulk reactivity in polycrystalline ice requires extensive information on the properties of the condensed aqueous phase confined at the GB's. Such information includes: the GB's dimensions at various temperatures; the transport properties of GB's, i.e., the diffusivity of water and other chemical species along the GB's; and the reactivity of water and other chemical species confined to microscopic dimensions characteristic of grain boundaries. Although the surface and bulk properties of single crystal ice have been the subject of many past experimental studies, the GB phenomena in ice have remained relatively unexplored.

Lack of experimental investigations of the ice grain boundary phenomena can be explained by numerous challenges involved in studies of these condensed aqueous phase systems. Naturally occurring ice samples, as well as those grown in the laboratory, are usually characterized by a large average grain sizes, which makes it difficult to distinguish between processes at the grain boundaries and in the crystallites. Furthermore, there are very few experimental techniques which facilitate real-time, *in situ* interrogations of molecular transport and chemical reactions in the bulk of ice near its melting point.

Using a novel experimental approach, fast thermal desorption spectroscopy (FTDS)[22-24], we were able to overcome many of the challenges involved in studies of physical and chemical phenomena at grain boundaries in polycrystalline ice. The central idea of our experimental approach is simple and reminiscent of the desorption experiments conducted by Langmuir[31]. At the core of our experimental setup is a thin, 10 micrometers in diameter, tungsten filament positioned in a vacuum chamber and initially set at temperatures below -150 °C. At this temperature, a few micrometer thick amorphous solid water (ASW) films doped with a variety of chemical species can be grown on the filament by vapor deposition. Following the deposition, the film is rapidly (over a fraction of a millisecond) heated to a value near 0 °C by passing electrical current through the filament. During the heating stage of the experiments, the ASW film crystallizes which results in a polycrystalline ice sample characterized by extremely small (less than 30 nm) average grain size. The heating and crystallization is followed by nearly isothermal vaporization of the film at temperatures near 0 °C. During the isothermal vaporization stage of the experiments, the flux of species evolving from the polycrystalline ice film is monitored with a mass spectrometer, thus, making it possible to directly observe the progress of a reaction in its bulk.

Recently, we conducted series of FTDS experiments with sandwich-like $H_2O/D_2O/H_2O$ ice films. The main objective of these studies was to infer water self-diffusion coefficients in polycrystalline ice near 0 °C from the kinetics of H/D exchange between H_2O and D_2O layers. While in our previous article[24] we

report estimates of the absolute values of water self-diffusion coefficients at grain boundaries at a single temperature of -2 °C, the focus of the current work is the temperature dependence of water diffusivity in pure polycrystalline ice and in polycrystalline ice doped with HCl. As we describe in the following sections of this article, comparison between temperature dependence of self diffusion in pure and doped ice makes it possible to gain significant insights into structure, transport properties, and possible phase transitions in a confined aqueous phase at grain boundaries. We hope that in addition to its fundamental value, essential conclusions of this work may be of interest to researchers in the field of environmental science.

II. EXPERIMENTAL

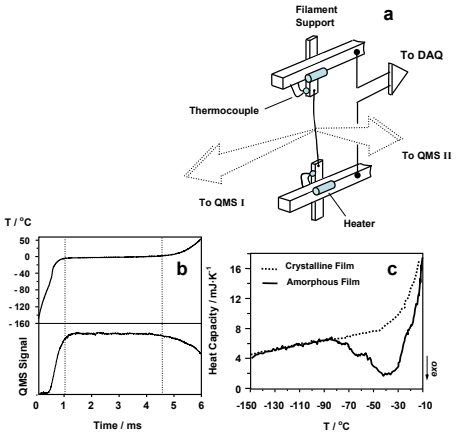

Figure 1

A detailed description of the FTDS apparatus and standard experimental procedures can be found elsewhere[22-24]; therefore, only a brief account is provided here. As shown in Figure 1a, ice films are grown on the surface of a tungsten filament (10 μm in diameter, 2 cm long), which is spot-welded to the supports of the filament assembly. The supports, while in thermal contact with the liquid nitrogen-cooled heat sink, are electrically isolated from the rest of the apparatus. The filament assembly includes a thermal control system capable of maintaining the filament supports at temperatures ranging from -160 °C to -120 °C. The assembly is surrounded by cryogenic shields (not shown) and positioned in a vacuum chamber pumped with a 2500 $L \cdot s^{-1}$ Varian diffusion pump. The chamber is maintained at pressures below $3 \cdot 10^{-7}$ Torr, during all stages of FTDS experiments.

Water vapors (H_2O^{16}, H_2O^{18}, and D_2O) are delivered from the vapor source to the filament via an array of effusive dosers, which consist of 12 stainless steel tubes with an 1/8'' diameter. The dosers are equally spaced around the filament at a distance of approximately 5 cm from its center (not shown in Fig. 1a). The intersecting vapor beams from the dosers lead to the formation of a relatively dense water vapor cloud around the tungsten filament and, thus, facilitates the deposition of uniform ice films with a neat cylindrical geometry and thickness of up to 4000 nm at a rate of 1 to 50 nm/s.

After deposition, rapid, nearly *isothermal* desorption of the film is initiated by applying a 2V – 5V potential difference across the filament. In the course of the entire FTDS experiment, the voltage across the filament and the current through the filament are recorded every four microseconds by a custom designed data acquisition system. The effective resistance values are calculated from current and voltage data according to Ohm's law. The temperature is then calculated from the resistance data using the temperature coefficient of electrical resistivity of tungsten (0.0045 $°C^{-1}$). A calibration procedure, based on the melting of micrometer thick polycrystalline ice films, was routinely performed to ensure the ± 1.5 °C overall accuracy of filament temperature measurements[22].

During rapid desorption of the film, the flux of vaporization products is analyzed simultaneously with three different types of detectors. First, a fast ionization gauge (FIG) is used to monitor the overall vaporization kinetics of the films. The FIG was positioned 6 cm away from the filament behind a centimeter-wide slit cut between cryogenic shields. Second, the vaporization products are analyzed with a quadrupole mass spectrometer situated approximately 10 cm away from the filament (QMS-1) inside a differentially pumped vacuum chamber[23,24]. Finally, in selected experiments, the velocity distributions of vaporization products were studied with a time-of-flight (TOF) arrangement, which utilized a sensitive

quadrupole mass spectrometer (QMS-2), and a rotating chopper wheel. The QMS-2 was positioned inside a doubly differentially pumped chamber at approximately one meter away from the filament[22].

Figure 1b illustrates the typical data obtained in a FTDS experiment. It shows the H_2O flux from the filament and the corresponding temperature of the filament. The H_2O flux was measured with the QMS-1. As shown in the Fig. 1b, a rapid rise in the temperature of the filament during the first millisecond of the FTDS experiment is followed by a region of relative thermal stability. Indeed, examination of the temperature data after 1 ms demonstrates that the temperature of the filament increases by less than 2 °C during the next several milliseconds of the desorption experiment. Achieving a steady state temperature coincides with the onset of H_2O desorption.

The steady-state vaporization regime can be rationalized in the following way: the heat generated by filament leads to rapid increase in temperature during initial stage of the experiment. However, at temperatures above -100 °C, resistive heating of the filament is counteracted by cooling due to vaporization. Thus, a dynamic equilibrium is achieved at a temperature where the vaporization rate of ice is sufficiently high so that the power generated by the filament is equal to the heat flux from the surface of the filament due to vaporization of the ice film.

Due to its cylindrical geometry, the evaporation of ice results in gradual decrease in the surface area of the film during steady-state evaporation. However, a gradual decrease in the surface area also leads to an increase in the temperature of the filament due to a lower cooling efficiency. Because of a strong Arrhenius dependence of the vaporization rate on temperatures, this drift in temperature is less than a few degrees. Although not immediately apparent in Fig. 1b, the temperature of the filament indeed increases slowly from -5 to -3 ^{o}C during steady-state vaporization of a few micrometer thick ice films. However, careful examination of the power, temperature, and vaporization data shows that vaporization of the ice samples is consistent with zero-order desorption kinetics.

Observation of zero-order desorption kinetics leads to several important conclusions. First, during isothermal desorption near 0 °C, the ice adlayer on the surface of the filament is a neat film free of *large* pores or ruptures, i.e., the film covers the entire filament surface[22]. Second, the temperature gradient *along* the length of the filament is negligible except within a fraction of a millimeter near the ends of the filament[22]. Finally, since the temperature of the filament does not vary significantly with the film thickness during vaporization, the temperature gradient in the film must be less than a few degrees[22]. Note that in the past, we also used data from the TOF experiments to characterize thermal gradients across the bulk of vaporizing D_2O ice films[22]. In these experiments, the temperature of the ice *surface* was determined by fitting Maxwellian distributions to the experimental TOF spectra and was compared to the temperature of the filament derived from resistance measurements. The temperature values obtained by these two methods were equal within the experimental errors (± 3 °C), thus, proving that the temperature gradients in FTDS experiments are, indeed, small.

Mass, thickness, and phase composition of our ice samples were determined by an ultrafast microcalorimetry technique[24,25]. In these experiments, the combined effective heat capacity of the ice film and the filament was calculated as the ratio of the power generated by the filament to the first time derivative of the temperature. Figure 1c illustrates the typical results. The solid line shows the effective heat capacity of the filament with a H_2O film vapor-deposited at -150 °C, and the dotted line shows the effective heat capacity of the filament with a H_2O film vapor-deposited at -150 °C and then annealed at temperatures near -10 °C for a fraction of a millisecond. In the case of the annealed film, the monotonic increase in heat capacity of the filament-film system, *i.e.*, the lack of exothermic transitions characteristic of crystallization, demonstrates that the ice sample is crystalline. However, in the case of the film deposited at -150 °C, the effective heat capacity shows partially overlapping irreversible exotherms, which we attribute to crystallization of the initially amorphous ice sample[22,25]. Assignment of the

exotherms shown in Fig. 1c to crystallization of amorphous ice is facilitated by approximately 2 kJ/mol enthalpy release, which is close to previously reported values[25]. These calorimetric experiments also show that non-crystalline ice films always undergo crystallization before steady state vaporization can occur at temperatures above -25 °C. Assuming that a *crystallized* film has the specific heat capacity and density of hexagonal ice, the estimate of the total mass of the film can be obtained by simply dividing the total heat capacity of ice film by the specific heat capacity of hexagonal ice. Using the mass of the ice film and assuming that ice film geometry is close to that of a neat cylinder, we routinely determine the thickness of our films with accuracy of ± 10%[24].

III. RESULTS

A. FTD spectra of D_2O and HDO in the case of pure ice

Figure 2 shows the fast thermal desorption (FTD) spectra of D_2O and HDO from 3.5 micrometer thick $H_2O/D_2O/H_2O$ ice films undergoing vaporization at a near constant temperature of -1 ± 1 °C. The sandwich-like $H_2O/D_2O/H_2O$ films were grown by vapor deposition on the filament's surface at -155 °C. The low deposition temperature minimized the reaction between D_2O and H_2O, during film deposition. After the deposition, the films were heated with an average rate in excess of 10^5 K/s to a temperature near ice melting point. Based on the thermogram measured during this rapid temperature rise, the initially amorphous $H_2O/D_2O/H_2O$ film underwent a complete crystallization at temperatures near -60 °C. The effective thickness of the *crystalline* D_2O layers was estimated as 350 ± 15 nm.

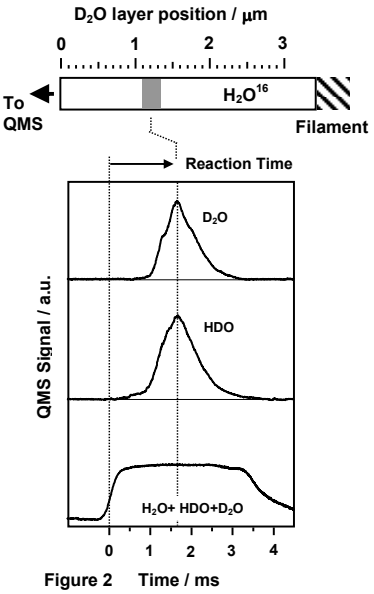

Figure 2

As shown in Fig. 2, a layer of D_2O, initially positioned at a distance of 1.2 micrometers away from the film's surface, evolves from the ice film only after vaporization of the overlying H_2Olayer. The time interval from the onset of H_2O vaporization to the appearance of the D_2O vaporization peak, or the mean residence time of D_2O in the bulk of the H_2O film, gives the mean reaction time for H_2O/D_2O isotopic exchange. Integration of the FTD spectra in Fig. 2 demonstrates that approximately 25% of the initial amount of D_2O is converted to HDO over the time span of approximately 1.7 ms, when the vaporization of the film occurs near -1 °C.

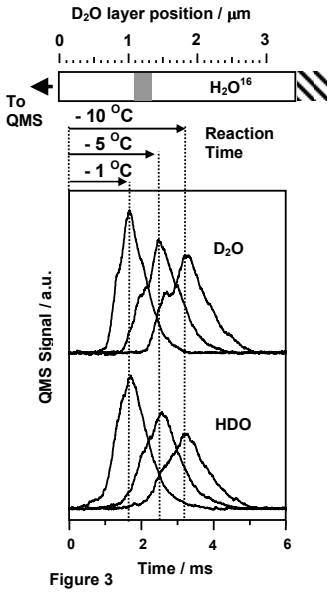

Figure 3

Both the HDO and the D_2O FTD spectra in Fig. 2 are broad and consist of two distinct features: a weak shoulder at 1.2 ms and a peak at 1.8 ms. As described in our previous article[23], the shoulder in the isothermal desorption spectra of HDO, and D_2O represents the vaporization of tracer species residing at or near the grain boundaries; whereas, the peak corresponds to the vaporization of tracer species incorporated into the crystallites of the polycrystalline H_2O ice film. Although an analysis of a FTD spectrum *shape* may, in principle, provide information on the diffusivity of the tracer species in the bulk of the polycrystalline H_2O ice film, such an analysis would be complicated by the surface morphological dynamics and TOF broadening[23]. Therefore, our investigations of molecular transport in polycrystalline ice were based primarily on studies of the H/D exchange kinetics, which was accomplished by integration of FTD spectra of HDO and D_2O measured at various temperatures.

Figure 3 presents FTD spectra of D_2O and HDO obtained at temperatures ranging from -10 to -1 °C. The initial position of the D_2O layer in the bulk of H_2O film (see the top panel in Fig. 3) was 1.2 micrometers away from the

surface in all experiments. The thickness of the D_2O layer was the same in all experiments and equal to approximately 350 nm. As shown in Fig. 3, lowering the temperature of isothermal desorption leads to an increase in the residence time of D_2O due to slower vaporization of the overlaying H_2O layer at lower temperatures. However, a cursory comparison of the desorption spectra in Fig.3 indicates that the amount of HDO in the isotopic exchange reaction decreases with temperature in spite of the longer mean reaction time. The decrease in the HDO yield at lower temperatures, which occurs despite longer reaction times, implies a strong dependence of the rate of H_2O/D_2O interdiffusion on temperature.

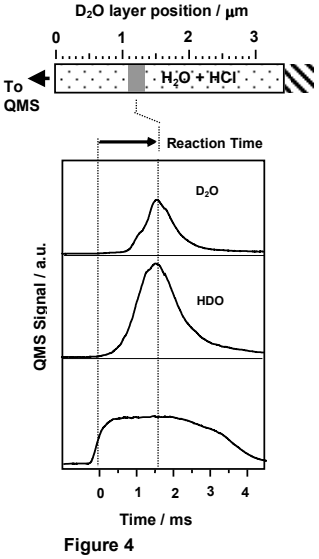

Figure 4

B. FTD spectra of D_2O and HDO in the case of doped ice.

The primary goal of the experiments described in this article was to gain insights into structure, transport properties, and possible phase transitions in a confined aqueous phase at grain boundaries in *pure* polycrystalline ice. This goal is best accomplished through comparison of the results from FTDS studies of pure ice with those of ice doped with chemical species which ionize in polycrystalline ice even at cryogenic temperatures. A well-studied example of such species is hydrogen chloride (HCl), which undergoes dissociation on surface ice at temperatures perhaps as low as 120 K[26]. In addition to serving as practical means for achieving the primary objective of our FTDS studies, the experimental results with HCl may also be of general fundamental and applied interest due to abundance of these species in the atmosphere[26].

Figure 4 shows the fast thermal desorption spectra of polycrystalline ice doped with HCl. Doped polycrystalline ice films used in these experiments were prepared exactly as described in the previous section with one exception: during H_2O and D_2O deposition the filament chamber was pressurized to $5\cdot10^{-7}$ Torr with 5% mixture of HCl and helium gases (Spectrogases). According to the mass spectroscopic analysis of flash desorption spectra, concentration of HCl in the resulting doped films was on the order of $(2\pm1)\cdot10^{-4}$ (mole fraction), or approximately 0.04 % by mass.

Comparison of data in Fig. 2 and 4 shows significant differences between the FTD spectra in the case of doped and pure polycrystalline ice. First, the ratio of HDO and D_2O yields in the case of doped polycrystalline ice is much greater than that in the case of pure ice. Second, the width of the HDO isothermal desorption spectrum in the case of doped ice is greater than that in the case of pure ice. Both of these observations imply a greater interdiffusion rate between H_2O and D_2O layers in ice seeded with HCl.

Figure 5 shows the temperature dependence of the HDO and D_2O spectra in the case of doped ice. Once again lowering the temperature of isothermal desorption leads to shift in HDO and D_2O vaporization spectra toward longer times, i.e., results in longer residence/reaction time due to slower vaporization of the overlaying H_2O at lower temperatures. Unlike the data presented in Figure 4, the amount of HDO produced in the H/D exchange reaction exceeds significantly the amount of unreacted D_2O at any temperature. FTD spectra of HDO in Fig. 5 are also significantly broader those in Fig. 4.

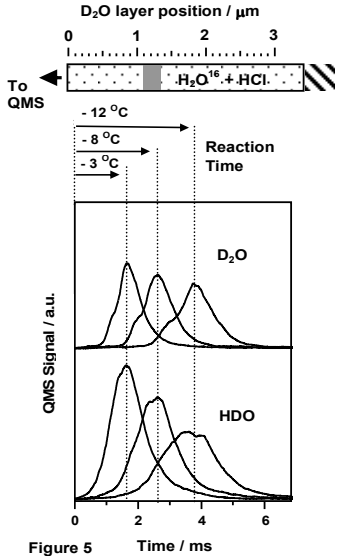

Figure 5

C. Analysis of FTD spectra.

The fast thermal desorption spectra shown in Figure 3 and 5 contain a wealth of information on the transport properties of polycrystalline ice at temperatures near its melting point. In our previous article[24],

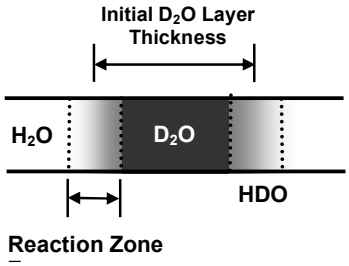

Figure 6

we described the results of FTDS experiments conducted at a single vaporization temperature of -2 °C. In particular, we studied dependence of HDO and D_2O yields on the initial thickness of the D_2O layer. From these studies, the following qualitative view of interactions between D_2O and H_2O layers in polycrystalline $H_2O/D_2O/H_2O$ films emerged:

1. When not limited by molecular diffusion of H_2O and D_2O, the H/D exchange in pure polycrystalline ice is rapid, resulting in complete conversion of a few nanometer thick D_2O film to HDO on a sub-millisecond time scale.

2. As shown in Fig. 6, when the initial thickness of the D_2O layer is on the order of a few hundred nanometers, the H/D exchange in polycrystalline ice films is confined to relatively narrow reaction zones at the interfaces between the H_2O and D_2O layers. The effective width of the reaction zone is determined by the extent of interdiffusion between the H_2O and D_2O layers over the mean reaction time.

3. HDO yield from the reaction between the D_2O and H_2O layers is proportional to the effective width of the reaction zone.

Taking into account the results of our earlier experiments, we arrive at a simple method for gauging the relative magnitude of the *effective* water self-diffusion coefficients in polycrystalline ice at various temperatures. Since the HDO yield, is proportional to the width of the reaction zone, i.e., to the effective length scale of the H_2O/D_2O interdiffusion in polycrystalline ice, the effective water self-diffusivity, D_{eff}, can be estimated as

where Y_{HDO} is the relative HDO yield, which can be calculated by integrating a FTD spectrum over isothermal vaporization time, and t_R is the mean reaction time.

Although Eq. 1, which is essentially the Einstein-Smoluchowski relation, is unlikely to provide a correct description of the molecular transport in inhomogeneous polycrystalline ice films, it makes it possible to summarize the results of the FTDS experiments in a comprehensive way. Furthermore, as we discuss immediately below, the deviations of the D_{eff} from the Arrhenius dependence on temperature allow significant insights into the physical properties of the aqueous phase at the grain boundaries in our polycrystalline ice films.

D. Effective water self-diffusion coefficients.

The effective water self-diffusion coefficients, D_{eff}, calculated for various temperatures using Eq. 1 in the case of pure and doped polycrystalline ice films are shown in Fig. 7. As we already explained, the HDO

$$D_{eff} \sim \frac{Y_{HDO}^{\,2}}{t_R} \qquad (1)$$

yields were obtained by integrating the corresponding HDO FTD spectra over the vaporization time. The absolute values of water self diffusion coefficients were estimated by using results of our previous FTD experiments, where a quantitative relationship between the HDO yield and the width of the reaction zone was established[24]. According to this study the D_{eff} in the case of pure polycrystalline ice was $10^{-4\pm0.25}$ $\mu m^2 \cdot ms^{-1}$ at -2 ± 1.5 °C. Because the conditions of FTDS experiments described in this article were essentially the same as in our previous study[24], the absolute value of the water self diffusion coefficient at -2 °C can be used to estimate the absolute value of D_{eff} at other temperatures.

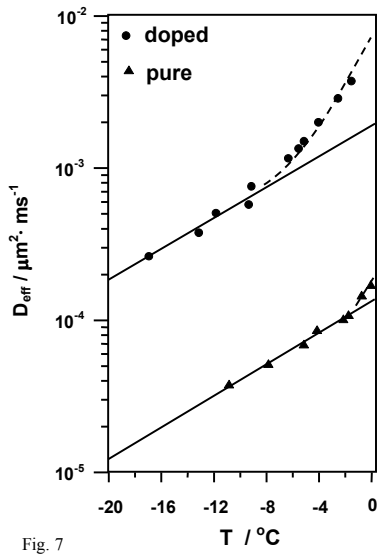

Fig. 7

As shown in Fig. 7, in the case of *pure* polycrystalline ice, the D_{eff} dependence on temperature is consistent with the Arrhenius law up to -2 °C. The effective activation energy, E_{eff}, obtained from Arrhenius fit of D_{eff} values in this temperature range, is 69 ± 3 kJ·mol^{-1}, i.e., is near the activation energy for water self diffusion in single crystal ice determined by George and coworkers in experiments with vapor deposited ice films at cryogenic temperatures (approximately 70 kJ·mol^{-1})[27]. The diffusion pre-exponential, D_0, is $5 \cdot 10^{9\pm0.6}$ μm^2·ms^{-1}. The absolute values of D_{eff} obtained in FTDS experiments are, on average, 10-100 times greater than those measured in previous experiments with macroscopic ice *single crystals* at temperatures near the melting point[28,29]. We note that low temperature studies[27] of HDO diffusivity in ultrathin (presumably single crystal) ice films resulted in D_{eff} values, which were also approximately two orders of magnitude greater than the water self-diffusivity values extrapolated from data obtained with macroscopic single crystal ice sample.

In the case of polycrystalline ice doped with HCl, the water self-diffusion coefficients are from one to two orders of magnitude greater that those for pure polycrystalline ice, and, consequently, 100-1000 times greater than those in pure single crystal ice. We note that this result is also consistent with low temperature measurements of diffusivity in doped single crystal ice by George and coworkers[27]. Furthermore, unlike D_{eff} in pure ice, water self-diffusivity in polycrystalline ice doped with HCl shows a more complex dependence on temperature. As shown in Fig. 7, the E_{eff} for water self diffusion in doped polycrystalline ice is close to 70 kJ·mol^{-1} at temperatures below -8 °C. However, it nearly doubles at higher temperatures.

IV. DISCUSSION

A. Diffusive regime

In order to interpret the observed dependences of D_{eff} on temperature, we must first determine the correct

$$L \approx (\delta D_{gb})^{1/2} \cdot (t/D_c)^{1/4} \qquad (2)$$

theoretical model for description of transport phenomena in polycrystalline ice under conditions characteristic of our FTDS experiments. As we explained in the previous section, our analysis of water self-diffusivity in polycrystalline ice relies on the estimate of the width of the reaction zone, L, which is determined by the rate of intermixing of D_2O and H_2O at the interface of two isotopically distinct regions in polycrystalline ice. In other words, our experimental arrangement is essentially a diffusion couple, where the characteristic *penetration depth* is the width of the reaction zone. Although it formally follows from the Eq. 1 that L is a simple function of an effective diffusion coefficient, we emphasize that, in general, the penetration depth may be a function of the following parameters: the diffusion coefficient at the grain boundaries, D_{gb}; the diffusion coefficient in the crystallites, D_c; the average crystallite size, G; the grain boundary width, δ; and the "annealing time", t, which is the average reaction time for H/D exchange in our FTDS experiments[30]. Depending on the relative magnitude of these parameters, a different theoretical description of the diffusion process in inhomogeneous polycrystalline media must be applied. For example, when $\delta << (D_c \cdot t)^{1/2} << G$ B-regime occurs, and the effective penetration depth can be estimated as[30]

However, when $G << (D_c \cdot t)^{1/2}$ diffusion is in A-regime[30], which is characterized by a different relationship between various parameters of the polycrystalline solid:

$$L \approx (\varepsilon_c \cdot D_c \cdot t + \varepsilon_{gb} \cdot D_{gb} \cdot t)^{1/2}, \qquad (3)$$

where ε_c and ε_{gb} are the volume fractions of crystallites and grain boundaries in the bulk of a polycrystalline material, respectively. Note that the expression in the brackets in Equation 3 is essentially $D_{eff} \cdot t$, where D_{eff}, the effective diffusion coefficient, is given by the Hart-Mortlock equation[30], i.e., by a linear combination of diffusion coefficient along the grain boundaries and the diffusion coefficient in the crystallites.

Despite the uncertainties in values of the parameters in Eq. 2 and 3, we can still gain insights into the molecular transport at grain boundaries by using these equations in analysis of observed temperature dependence of the HDO yield. First, we must determine the diffusive regime characteristic of our experimental conditions. We begin with assuming that water self-diffusion in polycrystalline ice under conditions characteristic of our experiment follows the B-regime. Substituting expression for L given by Eq. 2 into Eq. 1, and taking the logarithm of both sides of the resulting equation, the following relationship between various activation energies involved in the diffusion-vaporization process can be obtained:

$$E_{eff} = E_{gb} - \tfrac{1}{2} E_c - \tfrac{1}{2} E_{vap} \qquad (4)$$

where E_{gb} and E_c are the activation energies for water self-diffusion along the grain boundaries and in the crystallites of the polycrystalline sample, respectively, and E_{vap} is the activation energy for vaporization of the polycrystalline ice. The later term in the Eq. 4 arises from temperature dependence of the mean reaction time, which is inversely proportional to the zero-order vaporization rate of the polycrystalline ice film. Note that the value of E_{vap} at temperatures near 0 °C was only recently determined in FTDS studies of the absolute vaporization rate of ice[22,23].

Combining the known values of E_c and E_{vap} (approximately 70, and 48 kJ· mol^{-1}) with the value of E_{eff} derived from the D_{eff} data in the case of pure polycrystalline ice, we can estimate the activation energy for water self-diffusion along impurity-free grain boundaries. Thus, under assumption of the B-diffusive regime, the E_{gb} is approximately 130 kJ· mol^{-1}, which is significantly greater than the activation energy for water self-diffusion in *single crystal ice*. Such high value of the activation energy for diffusion along defect-rich grain boundaries indicates that diffusion in our polycrystalline samples is *not* in the B-regime and a different theoretical description of the molecular transport must be used. By exclusion[31], we conclude that the microstructure and transport properties of our samples result in the A-diffusive regime[30]. Immediately below we give additional arguments in support of this conclusion.

As we described in the experimental section of this article, our polycrystalline ice sample are obtained by homogeneous crystallization of initially amorphous ice films during rapid heating. Although crystallization of our amorphous ice is complete prior to the onset of near isothermal vaporization, due to a short time scale of FTDS experiments (a few milliseconds), only a limited growth of the crystalline ice nuclei is expected during isothermal vaporization of the film. Assuming that the average diameter of the initial crystalline nuclei is on the order of a few nanometers, we can estimate the maximum size of the crystallites during vaporization of the film, by taking advantage of availability of experimentally determined ice grain growth constants[32]. Such an estimate results in a value of less than 30 nanometers for the average diameter of crystalline grains in our polycrystalline films[24].

Small grain dimensions of polycrystalline material is a prerequisite of A-type of diffusion, which arises when the mean diffusive length in single crystal material is greater than the average size of the crystallites on the time scale of an experiment, i.e., when $G << (D_c \cdot t)^{1/2}$. Taking into account the fact that the D_c in nanoscale crystallites may be as high as 10^{-4} μm^2·ms^{-1}, and that the average grain diameter may be somewhat smaller than our *upper* estimate of 30 nm, it is *not* surprising that the A-type theoretical formalism provides a correct description of the diffusion in our polycrystalline ice. The failure of the analysis based on Eq. 2, which requires mean diffusive length in single crystal to be significantly smaller than the average crystallite diameter, to provide a realistic estimate of the activation energy for water self

diffusion along impurity- free grain boundaries further strengthens this conclusion. Note that in doped ice, the A-diffusive regime is even more likely because the average crystallite size is expected to be smaller than that in pure due to a decrease in the crystallite growth rate[32].

B. Molecular transport and phase transition at grain boundaries in pure polycrystalline ice.

Having identified the A-regime as the most probable diffusive regime under our experimental conditions, we can continue with a quantitative analysis of D_{eff} data in Fig. 7. As it follows from Eq. 3, during the A-type diffusion process, D_{eff} is simply a linear combination of two diffusion coefficients, i.e., the coefficient of water self diffusion along the grain boundaries, D_{gb}, and in the crystallites, D_c:

$$D_{eff} \approx \varepsilon_c \cdot D_c + \varepsilon_{gb} \cdot D_{gb} \qquad (5)$$

where ε_c and ε_{gb} are the volume fractions of polycrystalline ice sample occupied by crystallites and grain boundaries. Using Eq. 5, we attempted to determine the range of D_{gb} consistent with our experimental measurements of D_{eff} at various temperatures. The results of this analysis are summarized immediately below.

Although, the volume fraction of our polycrystalline ice sample occupied by grain boundaries could not be determined directly in our experiments, we can still estimate its lower limit. Indeed, the minimum grain boundary width must be on the order of a few molecular diameters, i.e., approximately 1-2 nanometers. Thus, taking into account the maximum average diameter of the grains (30 nm), we obtain a value of a few percent for the minimum grain boundary volume fraction. Combining this lower limit estimate of ε_{gb} with the lowest possible value of D_c, we can calculate the *maximum* value of D_{gb} at a particular temperature using Eq. 5.

Figure 8 shows the range of possible values of D_{gb} calculated for various temperatures (dashed lines). The water self-diffusion coefficients in single crystal ice[28,29] (cross-hatched region), and in liquid water[33] (solid line) are shown for comparison. The upper estimates of D_{gb} correspond to the effective grain boundary width of one nanometer, while the lower estimate assumes that the grain boundary width is on the order of 5 nm. The water self diffusion coefficient in crystallites was assumed to be equal to that in bulk single crystal ice. While estimates of D_{gb} at a particular temperature may differ by an orders of magnitude depending on the assumed grain boundary and crystallite dimensions, they are still several orders of magnitude *lower* than self-diffusivity in bulk water. Furthermore, according to the Arrhenius analysis of the grain boundary diffusivity data in Fig. 8, the effective activation energy of water self-diffusion along the grain boundaries is 69 ± 3 kJ·mol^{-1}, *i.e.*, near the greatest measured value for water self diffusion *in single crystal ice* (70 kJ·mol^{-1})[27], and much lower that the E_a in bulk water (25-30 kJ·mol^{-1})[33], or in the near surface "quasi-liquid layer" obtained in NMR experiments (23 kJ·mol^{-1})[34]. Also note that the activation energy for water self-diffusion along grain boundaries is much higher than that in near surface regions of ultra-thin ice at cryogenic temperatures[35-37]. Thus, an important conclusion follows: the inferred value of the effective activation energy for water self-diffusion along grain boundaries in fine polycrystalline ice excludes the possibility of the formation of liquid-like inclusions in the bulk of pure polycrystalline ice at temperatures up to -2 °C.

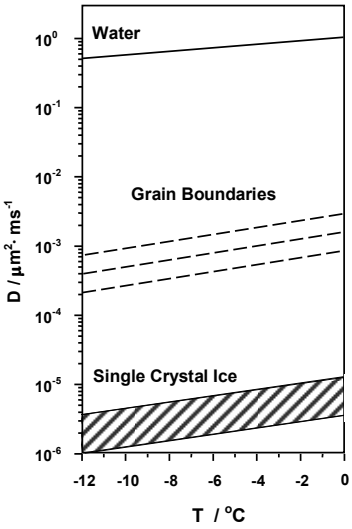

Figure 8

In the absence of grain boundary premelting, high apparent water self-diffusion coefficients at grain boundaries can be explained by two to four order increases in the density of interstitial, vacancy, or ionic defects at the interface between crystallites in the bulk of the polycrystalline ice sample. In other words, at temperatures as close to the melting point as two degrees, the grain boundaries in *pure* ice are neither liquid channels nor fissures in polycrystalline sample bulk. It also follows from the estimates of activation energy for water self-diffusion along the grain boundaries that the empirical rule, which postulates that activation energy for grain boundary diffusion is approximately 0.6 of that in single crystal[30], may not be true in the case of pure polycrystalline ice.

C. Molecular transport and phase transition at grain boundaries in doped polycrystalline ice.

Insights gained during analysis of water self-diffusivity data in the case of pure polycrystalline ice make interpretation of the observed temperature dependence of D_{eff} in the case of doped polycrystalline ice straightforward. The addition of HCl to vapor-deposited aqueous films must result in *inhibited* grain growth and a greater density of defects in the crystallites. As expected, a greater density of interstitial, vacancy, and ionic defects due to smaller grain size and impurities leads to an order of magnitude increase in the effective water self-diffusivity in doped polycrystalline samples. Nevertheless, at temperatures below -8 °C, the dependence of the D_{eff} on temperature demonstrates an apparent activation energy for water self diffusion, which is still nearly equal to the activation energy in single crystal ice.

At temperatures near -8 °C, the D_{eff} begins to deviate from Arrhenius law, which is manifested by a sudden increase in the apparent activation energy. In principle, the increase in the rate of the molecular transport observed at temperatures above -8 °C in the case of doped polycrystalline ice can be interpreted in two distinct ways. First, a rapid increase in the D_{eff} with temperature above -8 °C may signify the formation of liquid-like inclusions in the bulk of the polycrystalline ice, i.e., grain boundary premelting. Alternatively, such an increase may be rationalized by assuming a sudden activation of the proton transfer in "dry" polycrystalline ice at -8 °C in the presence of HCl. Because our measurements of the D_{eff} rely on the rate of the isotopic exchange between the H_2O and D_2O ice layers in the bulk of polycrystalline ice film, a sudden change in the mechanism of proton transport may appear as an increase in the molecular water self-diffusivity.

Although we are unable to provide unambiguous experimental evidence in favor of a particular hypothesis, we speculate that, in the case of doped polycrystalline ice, a grain boundary phase transition is more consistent with the observed variations of D_{eff} with temperature. Our arguments against a sudden activation of non-molecular proton transfer mechanism are based on two observations: first, we note that the deviation of D_{eff} from a simple Arrhenius dependence occurs gradually, i.e., there seems to be no apparent discontinuity in the data in Fig. 7. Second, as we already mentioned, the apparent activation energy at temperatures above -8 °C is almost twice of that in single crystal ice. Both of these observations seemed to be incompatible with the sudden proton hopping activation hypothesis. Indeed, if the mechanism of the proton migration suddenly changed from molecular interdiffusion of H_2O and D_2O to proton transfer by structural diffusion, a sudden increase in the rate of H/D exchange between the D_2O and H_2O layers would likely result in a "jump" in the apparent D_{eff} which would be followed by a slow increase with temperature, due to low activation energy characteristic of proton hopping[38].

In contrast to the sudden proton hopping activation mechanism, the grain boundary premelting provides a ready explanation for a monotonous, albeit non-Arrhenius, increase in D_{eff} in the case of doped ice. Depending on the concentration of ionic impurities, grain boundary premelting may occur gradually after an abrupt onset[39]. Thus, the contribution of a liquid-like component to the molecular transport in polycrystalline ice will also increase gradually with temperature. In order to demonstrate that a progressive grain boundary premelting may explain the observed dependence on D_{eff} on temperature in the case of doped polycrystalline ice, we used a simple model to fit the D_{eff} data obtained in our FTDS

experiments. According to this model, the D_{eff} in the case of doped ice is a liner combination of self-diffusion coefficient in "dry" doped polycrystalline ice, D_{ice}, and in bulk liquid water D_{water}, *i.e.*,

$$D_{eff} \approx (1-\varepsilon_{water}) \cdot D_{ice} + \varepsilon_{water} \cdot D_{water} \quad , \qquad (6)$$

where $\varepsilon_{water}(T)$ is the volume fraction of pre-melted ice, which increases monotonously with temperature. An empirical function, $A \cdot exp(-B/T)$, was used to model the dependence of ε_{water} on temperature. The water self-diffusion coefficient in doped polycrystalline ice at any temperature was assumed to be simply a factor of 10^3 greater than in single crystal ice, i.e., $D_{ice}(T) \approx 1000 \cdot D_c(T)$.

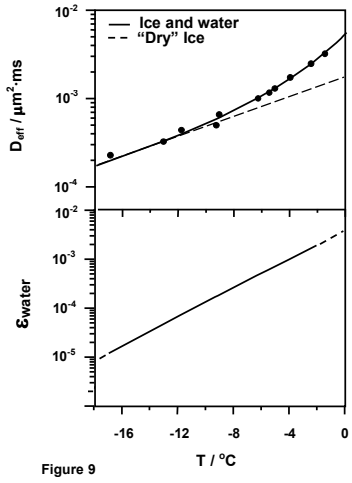

Figure 9

As shown in the upper panel of Fig. 9, the observed temperature dependence of D_{eff} is consistent with progressive premelting in the bulk of polycrystalline ice doped with HCl. The values of water volume fraction in doped polycrystalline ice samples at temperatures from -17 to -2 °C are shown in the lower panel of Fig. 9. According to the analysis, the formation of liquid-like inclusions, which occupy only a small (tenth of a percent) fraction of the overall volume of a polycrystalline ice sample, may result in a significant increase in the effective water self-diffusion coefficients. The strong effect of premelting on D_{eff} is due to large values of self-diffusivity in liquid water, which is assumed in our model of molecular transport in doped polycrystalline ice.

Although premelting in the bulk of polycrystalline ice doped with HCl provides a ready explanation for the observed dependence of D_{eff} on temperature, the small values of liquid-like volume fraction raise questions about possible morphology of liquid-like inclusions. For example, assuming that single crystal grains in our doped ice samples are "coated" with a thin layer of liquid, we can estimate the thickness of such layers as $\varepsilon_{water} \cdot R$, where R is the average effective radius of crystallites (less than 30 nm). Nevertheless, even at -2 °C, such an estimate results in the liquid-like layer thickness, which is significantly smaller than the thickness of a single monolayer of water. Thus, we arrive at an important conclusion: unless self-diffusivity in the premelted regions of polycrystalline ice is a few orders of magnitude less than that in water, premelting must occur predominantly along the grain boundary intersections forming a network of liquid-like veins in the bulk of polycrystalline film. The average diameter of such veins can be estimated as $(\varepsilon_{water})^{1/2} \cdot R$, and is consistent with values ranging from one to five nanometers in the temperature range between -17 and -2 °C.

V. SUMMARY AND CONCLUSIONS

The results of FTDS studies of temperature dependence of H/D exchange kinetics demonstrate that, in the limit of low concentration of impurities, grain boundaries do *not* undergo premelting at temperatures up to -2 °C. The effective water self-diffusion coefficient demonstrates an Arrhenius dependence on temperature. The high value of the activation energy (69 ±2 kJ·mol^{-1}) for water self-diffusion along grain boundaries inferred from H/D exchange data indicates that the diffusion mechanism at these interfaces is similar to that in single crystal ice. In terms of molecular transport, grain boundaries in a pure polycrystalline ice sample can be viewed simply as bulk ice characterized by a high density of interstitial and vacancy defects.

Addition of 0.04% (by mass) of HCl to polycrystalline ice sample results in one to two orders of magnitude increase in effective water self-diffusion coefficient. Furthermore, the temperature dependence of the effective water self-diffusion coefficient in polycrystalline ice indicates that unlike pure

polycrystalline ice, ice doped with HCl undergoes grain boundary premelting. Although the onset of premelting may occur at temperature as low as -8 °C, the volume fraction of liquid-like inclusion in the bulk of polycrystalline ice is relatively small even at temperatures near its normal melting point. Based on this, we conclude that premelting is likely to occur at grain boundary intersections forming a network of liquid-like veins in polycrystalline ice samples. According to our estimates, the average diameter of such veins is on the order of several nanometers. The results of experiments described in this article once again underscore the great potential of FTDS techniques in studies of molecular transport, phase transitions, and reactions in volatile polycrystalline materials.

ACKNOWLEDGEMENTS
We gratefully acknowledge the support from National Science Foundation (grant number 0416091) that made this study possible.

REFERENCES
1. J. S. Wettlaufer, in *Physics of Ice-Covered Seas*, edited by M. Leppranta, University of Helsinki Press, Helsinki, 1998.
2. J. W. Glen, D. R. Homer, and J. G. Paren, Int. Assoc. Sci. Hydrol., Publ. n62 118, 263, (1977).
3. J. G. Dash, Science, 246, 1591, (1989).
4. A. W. Rempel and M. G. Worster, J. Cryst. Growth 223, 420, (2001).
5. M. G. Worster and J. S. Wettlaufer, in *Fluid Dynamics at Interfaces*, edited by W. Shyy and R. Narayanan, Cambridge University Press, Cambridge, 1999.
6. H. P. Marshall, J. T. Harper, W. T. Pfeffer, and N. F. Humphrey, Geophys. Res. Lett., 29, 2146, (2002).
7. D. L. Goldsby, in *Glacier Science and Environmental Change*, edited by P. Knight, Blackwell, Malden, MA, 2006.
8. W. F. Weeks, in *Physics of Ice-Covered Seas*, edited by M. Leppranta, University of Helsinki Press, Helsinki, 1998, pp. 25–104.
9. P. B. Black, *Historical Perspectives of Frost Heave Research, Historical Perspectives in Frost Heave Research: The Early Works of S. Taber and G. Beskow*, edited by P. B. Black and M. J. Hardenberg, CRREL Special Report No. 91-23 (CRREL, Hanover, NH, 1991), p. 37.
10. R. Bindschadler, Science, 282, 428, (1998).
11. C. R. Bentley, Science, 275, 1077, (1997).
12. M. Oppenheimer, Nature, (London) 393, 325, (1998).
13. National Academy of Science, Sea-Level Change (National Academy Press, Washington, DC, 1990).
14. R. Zhang, M.-T. Leu, and M. Molina, Geophys. Res. Lett. 23, 1669, (1996).
15. K. S. Carslaw and T. Peter, Geophys. Res. Lett. 24, 1743, (1997).
16. R. Halde, Nuovo Cimento Soc. Ital. Fis., A 14, 575, (1980).
17. B. Chalmers, Sci. Am. 200(2), 114, (1959).
18. W. M. Elmore, "Water purification by natural freezing," M. Sc. thesis, University of Wyoming, 1968.
19. A. A. Chernov and A. M. Mel'nikova, Sov. Phys. Crystallogr. 10, 672, (1966).
20. A. W. Rempel, E. D. Waddington, J. S. Wettlaufer, and M. G. Worster, Nature (London) 411, 568, (2001).
21. I. Baker, D. Cullen, and D. I. Liescu, Can. J. Phys. **81**, 1, (2003).
22. V. Sadtchenko , M. Brindza , M. Chonde , B. Palmore , and R. Eom, J. Chem Phys., 121, 11980, (2004).
23. H. P. Lu, S. A. McCartney, M. Chonde , D. Smyla , and V. Sadtchenko, J Chem Phys., 125, 44709, (2006).
24. H. P. Lu, S. A. McCartney and V. Sadtchenko, J. Chem. Phys., 127, 184701, (2007).
25. M. Chonde , M. Brindza , and V. Sadtchenko, J. Chem. Phys., 125, 094501, (2006).
26. V. F. McNeill, F. M. Geiger, T. Loerting, B. L. Trout, L. T. Molina, and M. J. Molina, J. Phys. Chem. A, 111: 6274, (2007).
27. F. E. Livingston, J. A. Smith, and S. M. George, J. Phys. Chem. A, 106, 6309, (2002).

28. P. V. Hobbs, *Ice Physics,* Clarendon Press: Oxford, U.K., 1974.
29. V. F. Petrenko, and R. W. Whitworth, *Physics of Ice*, Oxford University Press: New York, 1999.
30. I. Kaur, Y. Mishin, and W. Gust, Fundamentals of Grain and Interphase Boundary Diffusion, Chichester, West Sussex: Wiley, (1995).
31. Note that C-diffusive regime is unlikely to be observed under conditions of our FTD experiments because the diffusion in ice crystallites cannot be completely disregarded at temperatures only a few degrees below ice melting point, which are typical for FTDS experiments. For discussion see Ref. 30.
32. For review see L. Arena, O. B. Nasello, and L. Levi, J. Phys. Chem. B 101, 6109, (1997).
33. H. R. Pruppacher J. Chem. Phys. 56, 101, (1972).
34. N. Materer, U. Starke, A. Barbieri, M. A. Van Hove, G. A. Somorjai, G. Kroes, and C. Minot, Surf. Sci., 381, 190, (1997).
35. K. H. Jung, S. C. Park, J. H. Kim, and H. Kang, J. Chem. Phys., 12*1*, 2758, (2004).
36. S. C. Park, K. H. Jung, and H. Kang, J. Chem. Phys., 121, 2765, (2004).
37. S. P. Oxley, C. M. Zahn, and C. J. Pursell, J. Phys. Chem. A, 110, 11064, (2006).
38. W. R. Groves, and C. H. Pennington, Chem. Phys., 315, 1, (2005).

39. L. Benatov, and J. S. Wettlaufer, Phys. Rev. E 70, 061606, (2004).

FIGURE CAPTIONS

Figure 1

The essentials of the fast thermal desorption spectroscopy (FTDS) apparatus and typical FTDS experimental data. (a) Polycrystalline ice films are deposited on a 10 μm in diameter and 2 cm long tungsten filament. The filament is spot welded to two supports, which are in thermal contact with a liquid-nitrogen-cooled heat sink. During ice film deposition, the temperature of the entire filament assembly can be varied from −160 to −100 °C by balancing heat flux from resistive heaters against heat loss to the LN sink. During ice film deposition, the temperature of the filament supports is monitored by two T-type thermocouples. Rapid vaporization of the film near 0 °C is initiated by a current pulse from a data acquisition (DAQ) system. The fluxes of vaporization/reaction products can be monitored by either of two quadruple mass spectrometers (QMSs), or a fast ionization gauge (FIG). The current through the filament, applied voltage, and the FIG and QMS signals are recorded by the DAQ system every 4μs. (b) Typical data obtained in a FTDS experiment. Upper panel: The temperature of the filament as a function of time. The temperature is calculated from resistance data. Lower panel: The overall vaporization flux from the filament as a function of time as measured with the FIG. (c) Typical fast scanning thermograms of amorphous (solid line) and polycrystalline (dashed line) ice samples. In the case of amorphous ice, the thermogram shows multiple exothermal transitions, which we attribute to relaxation of the amorphous ice and its consequent crystallization. The thermograms are inferred from current and voltage data measured during the initial heating of the ice samples in FTDS experiments. The effective heat capacities were calculated as a ratio of the power generated by the filament to the first time derivative of the filament's temperatures.

Figure 2

Fast thermal desorption spectra of D_2O and HDO from a 3.5 μm thick $H_2O/D_2O/H_2O$ film (upper and middle panels) measured at -1 ± 1 °C. The initial D_2O layer's position was approximately 1.2 μm away from the film's surface. The overall desorption kinetics of the film, monitored with the FIG, are shown for comparison (lower panel). The mean reaction time for the H/D isotopic exchange is defined as the mean residence time of D_2O in the bulk of the H_2O film, i.e., the time interval from the onset of H_2O vaporization up to the appearance of the D_2O vaporization peak in the thermal desorption spectrum.

Figure 3
FTD spectra of D_2O and HDO obtained at temperatures ranging from -10 to -1 ^oC in pure ice. The initial position of the D_2O layer in the bulk of H_2O film was 1.2 (top panel) micrometers away from the surface in all experiments. The thickness of the D_2O layer was the same in all experiments and equal to approximately 350 nm. Lowering temperature of isothermal desorption leads to increase in the residence time of D_2O due to slower vaporization of the overlaying H_2O at lower temperatures.

Figure 4
Fast thermal desorption spectra of polycrystalline ice doped with 0.04% of HCl (by mass). Comparison of data in Fig. 2 and 4 shows that the width of HDO isothermal desorption spectrum in the case of doped ice is greater than that in the case of pure ice, and that the ratio of HDO and D_2O yields in the case of doped polycrystalline ice is much greater than that in the case of pure ice. These observation point out to a significant increase in water self diffusion coefficient in HCl doped polycrystalline ice.

Figure 5

FTD spectra of D_2O and HDO obtained at temperatures ranging from -12 to -3 ^oC in polycrystalline ice doped with 0.04% HCl. The initial position of 350 nm thick D_2O layer in the bulk of H_2O film was 1.2 micrometers away from the ice film surface in all experiments (see top panel). Lowering temperature of isothermal desorption results in increase in the residence time of D_2O due to slower vaporization of the overlaying H_2O at lower temperatures. The amount of HDO produced in the H/D exchange reaction exceeds significantly the amount of unreacted D_2O at any temperatures.
Figure 6.

H/D exchange reactions in ice film. According to our previous studies (ref. 24) H/D exchange reactions occur on the interfaces of D_2O and H_2O layers. The effective width of the reaction zone is determined by the extent of inter-diffusion between H_2O and D_2O over the mean residence (reaction) time of D_2O layer in rapidly vaporizing ice film.

Figure 7

Effective water self-diffusion coefficients at various temperatures (D_{eff}), in pure and HCl-doped polycrystalline ice. Note that water self-diffusion coefficients in single crystal ice are approximately two orders of magnitude lower than those in our pure polycrystalline ice samples. In *pure* ice, D_{eff} dependence on temperature is consistent with the Arrhenius law up to -2 ^oC. The effective activation energy, E_{eff}, obtained from Arrhenius fit of D_{eff} values in this temperature range, is 69 ± 3 $kJ \cdot mol^{-1}$. In HCl-doped, D_{eff} demonstrates an Arrhenius-like dependence at low temperatures ($E_{eff} \approx 70$ kJ/mol). However, the apparent activation energy nearly doubles above near -8 ^oC. As described in the text, the deviation D_{eff} from Arrhenius dependence in the case of HCl –doped ice is likely to be caused by onset of grain boundary premelting.

Figure 8
Water self diffusion coefficients at grain boundaries (D_{gb}) in pure polycrystalline ice at various temperatures. The values were inferred from the overall effective diffusion coefficients (D_{eff}) assuming that water self-diffusion is in A-regime. The upper estimates of D_{gb} correspond to the minimum physically meaningful grain boundary width of one nanometer, while the lower estimate assumes that the grain boundary width is on the order of 5 nm. Assuming a greater grain boundary width results in D_{gb} values, which are nearly equal to D_{eff} in Fig. 7. The water self-diffusion coefficients in single crystal ice and in supercooled liquid water are shown for comparison.

Figure 9

Upper panel: analysis of the water self diffusivity data (dots) in the case of HCl-doped polycrystalline ice. The line shows the fit of the D_{eff} with an A-type diffusion model where D_{eff} is a linear combination of water self-diffusion coefficients in "dry" polycrystalline ice and in supercooled water. The contribution of water-like diffusivity to the overall effective diffusion coefficient was assumed proportional to the volume fraction of water (ε_{water}) formed in the bulk of dry polycrystalline ice due to premelting. *Lover panel:* The volume fraction of liquid (ε_{water}) in polycrystalline ice at various temperatures derived from the fit of D_{eff} with the diffusion model describe above.